Introducing essentially non-oscillatory stencil selection with subcell resolution into uncertainty quantification

By J. A. S. Witteveen AND G. Iaccarino

1. Motivation and objectives

The high sensitivities caused by discontinuities in probability space can be robustly approximated by reducing the polynomial degree locally to a piecewise linear interpolation in a multi-element Uncertainty Quantification (UQ) approach. In this context, two points are important to maintain a highly accurate solution despite the locally first degree approximation. First, the linear region should be kept as small as possible, using solution-adaptive refinement to concentrate the samples near the discontinuity. Second, the higher-degree interpolation should be maintained in the elements discretizing the smooth regions as close as possible to the discontinuity to remain higher-order accurate near the singularity. These two objectives are achieved here by introducing an Essentially Non-Oscillatory (ENO)–type stencil selection into the Simplex Stochastic Collocation (SSC) UQ method.

In problems where the location of a discontinuity in physical space is uncertain, however, adaptive refinement in probability space proves ineffective. For each point in physical space, the spatial discontinuity results in a jump at a different location in probability space. Uncertain discontinuity locations also result in staircase approximations for the mean and standard deviation fields that converge with first-order accuracy only. This leads to an underprediction of the maximum standard deviation as well. In a non-intrusive UQ approach, the staircase behavior is caused by the discontinuity locally crossing a sampling point in probability space and the lack of resolution of the discontinuity location in between the samples. Therefore, we also introduce the concept of subcell resolution into uncertainty quantification to achieve accurate approximations of uncertain spatial discontinuities.

The ENO scheme was developed by Harten & Osher (1987) as a robust spatial discretization in the Finite Volume Method (FVM) for deterministic Computational Fluid Dynamics (CFD). It achieves an essentially non-oscillatory approximation of the solution of hyperbolic conservation laws. Non-oscillatory means, in this context, that the number of local extrema in the solution does not increase with time. The ENO scheme obtains this property using an adaptive-stencil approach with a uniform polynomial degree for reconstructing the spatial fluxes. Each spatial cell X_j is assigned r stencils $\{S_{j,i}\}_{i=1}^{r}$ of degree p, all of which include the cell X_j itself. Out of this set of candidate stencils $\{S_{j,i}\}$, the stencil S_j is selected for cell X_j that results in the interpolation $w_j(x)$, which is smoothest in some sense based on an indicator of smoothness $\mathrm{IS}_{j,i}$. In this way, a cell next to a discontinuity is adaptively given a stencil consisting of the smooth part of the solution, which avoids Gibbs-like oscillations in physical space. Attention was paid to the efficient implementation of ENO schemes by Shu & Osher (1988).

The notion of subcell resolution in the ENO scheme originated from Harten (1989) to

prevent the smearing of contact discontinuities by FVM in physical space. It is based on the observation that the location of a discontinuity x_{disc} within the cell X_j can be derived from the cell-averaged value $\bar{w}_j$. The ENO interpolations, $w_{j-1}(x)$ and $w_{j+1}(x)$, of the cells to the left and the right of the discontinuous cell X_j are then extended to the approximate discontinuity location x_{disc} in X_j such that their integral matches the cell average $\bar{w}_j$. This allows for resolving discontinuities in the interior of cells instead of restricting them to the cell face locations. The concept can be extended to multiple spatial dimensions using the dimensional splitting approach.

ENO-type stencil selection with subcell resolution is here introduced in the SSC multi-element UQ method to obtain accurate approximations of the impact of uncertain spatial discontinuities in probability space. The SSC method (Witteveen & Iaccarino 2011*a*,*c*) is based on an adaptive simplex elements discretization in parameter space Ξ with sampling points at the vertexes of the simplexes. In the ENO reconstruction for each simplex element Ξ_j, r_j interpolation stencils $\{S_{j,i}\}_{i=1}^{r_j}$ of sampling points are constructed which contain the subdomain Ξ_j. The stencil S_j is then selected in such a way that the smoothest interpolation $w_j(\boldsymbol{\xi})$ with $\boldsymbol{\xi} \in \Xi$ is obtained. The non-uniform polynomial degree $p_{j,i}$ of the candidate stencils $S_{j,i}$, that are accepted by an extremum conserving limiter, is used here as the indicator of smoothness $\text{IS}_{j,i}$. A simplex Ξ_j near a discontinuity, therefore, achieves a higher-order approximation in the resulting SSC–ENO method by assigning Ξ_j an asymmetrical higher-degree interpolation stencil S_j that does not contain the discontinuity. The locally higher polynomial degree p_j leads also to lower values of the adaptive refinement measure in Ξ_j, which restricts the refinement more to the simplexes that contain the discontinuity.

The subcell resolution (SR) in the SSC–SR method is obtained by determining the location of the discontinuity $\boldsymbol{\xi}_{\text{disc}}$ in probability space from the discontinuity locations in physical space for each of the deterministic simulations. These physical discontinuity locations are interpolated in probability space to derive a relation for the location of the discontinuity $\boldsymbol{\xi}_{\text{disc}}$ in probability space as a function of the spatial coordinate x. For the response surface approximation in the cells in probability space that contain the discontinuity, the interpolations $w_j(\boldsymbol{\xi})$ of the neighboring cells Ξ_j are extended from both sides up to the predicted discontinuity location $\boldsymbol{\xi}_{\text{disc}}$. This leads to the sharp resolution of the jump in the interior of the cells in probability space without the need for adaptive sampling near the discontinuity. It also avoids the staircase approximation of the statistics because of the continuous dependence of the discontinuity location $\boldsymbol{\xi}_{\text{disc}}$ in probability space on the spatial coordinate x.

Abgrall (2010) and Barth (2011*a*) proposed extending FVM directly to discretize the combined physical and probability space using the ENO scheme. Since FVM was originally developed for the three-dimensional physical space, the application of FVM to these higher-dimensional probability spaces can, however, be inefficient because of the curse of dimensionality. Subcell resolution was proposed by Ghosh & Ghanem (2008) in the form of basis enrichment in the Polynomial Chaos (PC) expansion. Their approach is, however, based on integrating *a priori* knowledge about the discontinuity location by selecting appropriate enrichment functions. A solution for the staircase approximation of the statistics in case of uncertain spatial discontinuities was proposed by Barth (2011*b*) using image enhancement postprocessing techniques in a combined discretization of physical and probability space. Other multi-element UQ methods (Babuška *et al.* 2004; Le Maître *et al.* 2004; Wan & Karniadakis 2005) are based, for instance, on Stochastic Galerkin (SG) projections of PC expansions (Ghanem & Spanos 1991; Xiu & Karniadakis

2002) in each of the subdomains. The Stochastic Collocation (SC) approach (Babuška *et al.* 2007; Xiu & Hesthaven 2005) can also be used to construct the local polynomial approximations based on sampling at quadrature points in hypercube elements (Agarwal & Aluru 2009; Foo *et al.* 2008; Ma & Zabaras 2009).

The outline of this paper is as follows. The SSC method is briefly discussed in Section 2. The extensions of SSC to ENO-type stencil selection and subcell resolution are introduced in Sections 3 and 4, respectively. In Section 5, the numerical application to a shock tube problem with uncertainty in the location of the discontinuities is considered.

2. Simplex Stochastic Collocation

The SSC method (Witteveen & Iaccarino 2011*a*,*c*) is a non-intrusive multi-element UQ approach that discretizes the probability space of stochastic problems using a simplex tessellation of sampling points. Consider the following computational problem subject to n_ξ second-order random parameters $\boldsymbol{\xi} = \{\xi_1, \ldots, \xi_{n_\xi}\}$ in parameter space $\Xi \subset \mathbb{R}^{n_\xi}$

$$\mathcal{L}(\mathbf{x}, t, \boldsymbol{\xi}; u(\mathbf{x}, t, \boldsymbol{\xi})) = \mathcal{S}(\mathbf{x}, t, \boldsymbol{\xi}), \tag{2.1}$$

with output quantity of interest $u(\mathbf{x}, t, \boldsymbol{\xi})$, space $\mathbf{x}$, and time t. The latter two arguments are dropped from here on to simplify the notation. The response surface $u(\boldsymbol{\xi})$ is approximated by a piecewise polynomial function $w(\boldsymbol{\xi})$ using a PC expansion (Ghanem & Spanos 1991; Xiu & Karniadakis 2002) $w_j(\boldsymbol{\xi})$ in each of the simplexes Ξ_j

$$w_j(\boldsymbol{\xi}) = \sum_{i=0}^{P_j} c_{j,i} \boldsymbol{\Psi}_{j,i}(\boldsymbol{\xi}), \tag{2.2}$$

for $\boldsymbol{\xi} \in \Xi_j$, where $\boldsymbol{\Psi}_{j,i}$ are the basis polynomials, $c_{j,i}$ are the coefficients, and $P_j + 1 = (n_\xi + p_j)!/(n_\xi! p_j!)$ is the number of expansion terms, with p_j the local polynomial degree. The coefficients $c_{j,i}$ are computed by interpolating a stencil S_j out of the n_s samples $\mathbf{v} = \{v_1, \ldots, v_{n_\mathrm{s}}\}$, with $v_k = u(\boldsymbol{\xi}_k)$ and $k = 1, \ldots, n_\mathrm{s}$, at the sampling points $\boldsymbol{\xi}_k$ in the vertexes of the n_e simplexes Ξ_j with $j = 1, \ldots, n_\mathrm{e}$. Deterministic simulations of (2.1) for the samples v_k are considered that are computationally intensive compared to the polynomial interpolation, such as, for instance, complex CFD problems.

For a piecewise linear interpolation $w_j(\boldsymbol{\xi})$ with $p_j = 1$, the stencil $S_j = \{\boldsymbol{\xi}_{k_{j,0}}, \ldots, \boldsymbol{\xi}_{k_{j,N_j}}\}$ consists of the $N_j + 1 = n_\xi + 1$ vertexes of the simplex Ξ_j, with $k_{j,l} \in \{1, \ldots, n_\mathrm{s}\}$ for $j = 1, \ldots, n_\mathrm{e}$ and $l = 0, \ldots, N_j$. Higher-degree stencils S_j with $N_j \geq P_j$ are constructed by adding vertexes $\boldsymbol{\xi}_k$ of surrounding simplexes to the stencil according to a nearest-neighbor search based on the Euclidean distance to the center of the simplex Ξ_j in parameter space Ξ. The center of Ξ_j is defined as the average of the vertex locations of Ξ_j. We use $N_j = P_j$ here and the interpolation can be constructed using a least-squares approximation for $N_j > P_j$. The notation is visualized in Figure 1 for an example of a response surface approximation in a two-dimensional probability space with $n_\xi = 2$.

The polynomial degree p_j is chosen as high as possible with respect to the total number of available samples n_s with $N_j + 1 \leq n_\mathrm{s}$. The robustness of the interpolation $w_j(\boldsymbol{\xi})$ of the samples $\mathbf{v}_j = \{v_{k_{j,0}}, \ldots, v_{k_{j,n_\xi}}\}$ in the simplex Ξ_j is guaranteed by the Local Extremum Conserving (LEC) limiter that reduces the stencil size $N_j + 1$, and p_j, in case of overshoots until $w_j(\boldsymbol{\xi})$ satisfies

$$\min_{\boldsymbol{\xi} \in \Xi_j} w_j(\boldsymbol{\xi}) = \min \mathbf{v}_j \;\wedge\; \max_{\boldsymbol{\xi} \in \Xi_j} w_j(\boldsymbol{\xi}) = \max \mathbf{v}_j. \tag{2.3}$$

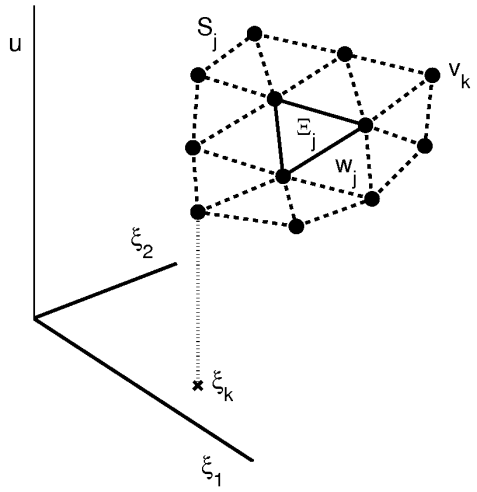

FIGURE 1. Approximation of the response surface $u(\boldsymbol{\xi})$ by the interpolation $w_j(\boldsymbol{\xi})$ of the samples v_k at a stencil S_j of sampling points $\boldsymbol{\xi}_k$ for the simplex Ξ_j in a two-dimensional probability space with $\boldsymbol{\xi} = \{\xi_1, \xi_2\}$.

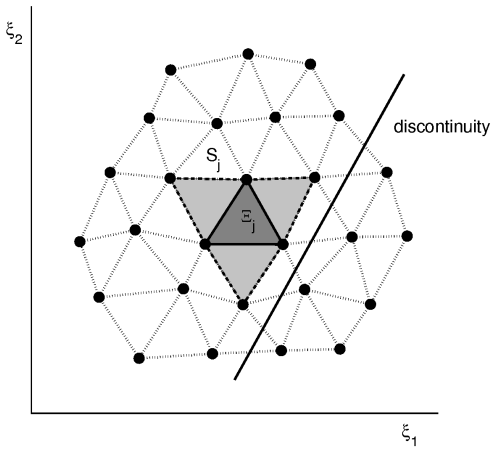

FIGURE 2. Nearest-neighbor interpolation stencil S_j for the simplex Ξ_j near a discontinuity in a two-dimensional probability space.

The LEC limiter (2.3) is applied to all simplexes in the stencil S_j and always holds for $p_j = 1$. For additional robustness, the polynomial degree can be reduced by one more order than that required by (2.3), if $p_j > 1$.

3. ENO stencil selection

An efficient algorithm for the SSC–ENO interpolation stencil selection is developed below. The implementation and the effect on the adaptive refinement are also discussed.

3.1. *Interpolation stencil selection*

The nearest-neighbor construction of the interpolation stencils S_j combined with the LEC limiter (2.3) results in one stencil S_j for each simplex Ξ_j. If the stencils S_j are not restricted to the nearest-neighbor sampling points $\boldsymbol{\xi}_k$, then multiple stencils $S_{j,i}$ may be possible for simplex Ξ_j that satisfy the LEC limiter. The stencil $S_{j,i}$ that leads to the smoothest interpolation $w_{j,i}(\boldsymbol{\xi})$ is then selected for a more accurate approximation of $u(\boldsymbol{\xi})$.

The first $n_\xi + 1$ sampling points $\boldsymbol{\xi}_k$ of each stencil $S_{j,i} = \{\boldsymbol{\xi}_{k_{j,0}}, \ldots, \boldsymbol{\xi}_{k_{j,n_\xi}}\}$ consist of the vertexes of the simplex Ξ_j. This stencil is equal to the stencil for piecewise linear interpolation of the previous section. The higher-degree stencils of $N_{j,i} + 1$ sampling points

$$S_{j,i} = \{\boldsymbol{\xi}_{k_{j,0}}, \ldots, \boldsymbol{\xi}_{k_{j,n_\xi}}, \ldots, \boldsymbol{\xi}_{k_{j,N_{j,i}}}\} \tag{3.1}$$

can be constructed by adding, in principle, any combination of $N_{j,i} - n_\xi$ samples for any $p_{j,i}$ out of the remaining sampling points $\boldsymbol{\xi}_k$, with $k \in \{1, \ldots, n_s\} \backslash \{k_{j,0}, \ldots, k_{j,n_\xi}\}$ and with each sampling point appearing only once in the stencil $S_{j,i}$. Out of these stencils, only a set of r_j candidate stencils $\{S_{j,i}\}_{i=1}^{r_j}$ is accepted, of which the interpolation $w_{j,i}(\boldsymbol{\xi})$

satisfies the LEC limiter. The stencil S_j for Ξ_j is selected from this set $\{S_{j,i}\}$ based on an indicator of smoothness $\mathrm{IS}_{j,i}$ for each of the candidates. Since the stencils $S_{j,i}$ have a non-uniform polynomial degree $p_{j,i}$, the degree is here used as the indicator of smoothness $\mathrm{IS}_{j,i} = p_{j,i}$. The stencil with the highest polynomial degree is then assigned to Ξ_j in order to obtain the highest order approximation

$$S_j = S_{j,i}, \qquad \text{with } i = \underset{i^* \in \{1,\dots,r_j\}}{\arg\max}\ p_{j,i^*}. \tag{3.2}$$

If multiple stencils have the same smoothness $p_{j,i}$, then out of these stencils the one with the minimum average Euclidean distance of the sampling points $\boldsymbol{\xi}_k$ to the center of Ξ_j is chosen.

A two-dimensional example is given in Figure 2 of the nearest-neighbor stencil for the simplex Ξ_j close to a discontinuity, of which the location is denoted by the diagonal line. The nearest-neighbor stencil S_j for Ξ_j only leads to a quadratic interpolation $w_j(\boldsymbol{\xi})$ with $N_j + 1 = 6$, since higher-degree stencils cross the discontinuity and are rejected by the LEC limiter. On the other hand, stencil selection can result in a stencil S_j, with a higher polynomial degree p_j, that contains all sampling points $\boldsymbol{\xi}_k$ in the smooth region at one side of the discontinuity (see Figure 3).

3.2. *Efficient implementation*

Constructing all possible stencils $S_{j,i}$ for all simplexes Ξ_j can become impractical as its complexity increases binomially with the number of samples n_s. Therefore, we restrict the stencil selection to a subset of these stencils by employing the multi-element character of the approach. We allow only nearest-neighbor stencils of other simplexes that contain Ξ_j to be assigned to the simplex Ξ_j, if that leads to a higher polynomial degree than its own stencil.

To that end, the nearest-neighbor stencils $\tilde{S}_j$, with interpolation $\tilde{w}_j(\boldsymbol{\xi})$ and degree $\tilde{p}_j$, are first constructed for each simplex Ξ_j, as described in Section 2. This results in a set of n_e stencils $\{\tilde{S}_j\}_{j=1}^{n_\mathrm{e}}$ for all simplexes Ξ_j. Next, it needs to be determined for each stencil $\tilde{S}_j$ which simplexes Ξ_i are part of the stencil. A stencil $\tilde{S}_j$ is considered to contain another simplex Ξ_i, if $\tilde{S}_j$ contains all vertexes $\{\boldsymbol{\xi}_{k_{i,0}}, \dots, \boldsymbol{\xi}_{k_{i,n_\xi}}\}$ of Ξ_i, which is always true for $i = j$. A set of $\tilde{r}_j$ candidate stencils $\{\tilde{S}_{j,i}\}_{i=1}^{\tilde{r}_j}$ for simplex Ξ_j is then collected from the nearest-neighbor stencils that contain Ξ_j. The stencil $S_j = \tilde{S}_{j,i}$, and the interpolation $w_j(\boldsymbol{\xi}) = \tilde{w}_{j,i}(\boldsymbol{\xi})$, with the highest degree $\tilde{p}_{j,i}$ is selected from $\{\tilde{S}_{j,i}\}_{i=1}^{\tilde{r}_j}$ as in (3.2). If none of the stencils $\{\tilde{S}_{j,i}\}$ has a higher-degree than that ofthe nearest-neighbor stencil $\tilde{S}_j$, i.e., $\tilde{p}_{j,i} \leq \tilde{p}_j$ for all $i = 1, \dots, \tilde{r}_j$, then the original stencil $\tilde{S}_j$ is automatically maintained, since the sampling points of the nearest-neighbor stencil have, by definition, the smallest average Euclidean distance to the center of Ξ_j.

This efficient SSC–ENO stencil selection algorithm results in virtually no additional computational costs compared to SSC with nearest-neighbor stencils, since no additional stencils or interpolations are constructed. Existing nearest-neighbor stencils are assigned only to other simplexes, if that increases the local polynomial degree. The algorithm can, therefore, only improve the polynomial degree, $p_j \geq \tilde{p}_j$, because $\{\tilde{S}_{j,i}\}$ always contains the stencil $\tilde{S}_j$.

Figure 4 shows the adoption of the nearest-neighbor stencil of another simplex Ξ_i by the simplex Ξ_j in the two-dimensional example. Because the resulting stencil S_j is asymmetrical with respect to Ξ_j, it leads to a higher polynomial degree p_j than its

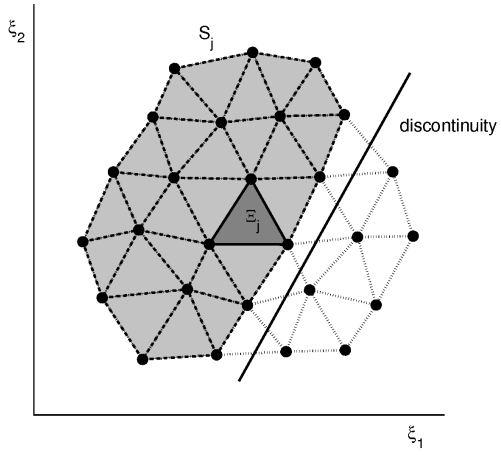

FIGURE 3. Selected interpolation stencil S_j for the simplex Ξ_j near a discontinuity in a two-dimensional probability space.

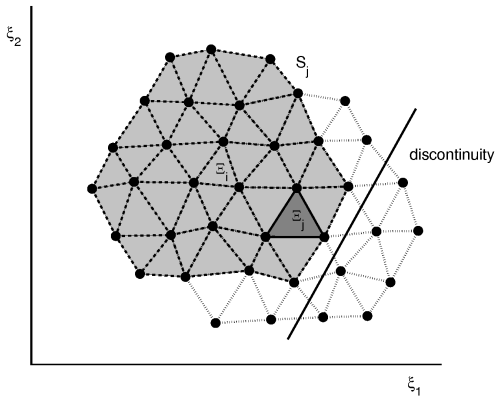

FIGURE 4. Efficiently selected interpolation stencil S_j for the simplex Ξ_j near a discontinuity in a two-dimensional probability space.

nearest-neighbor stencil of Figure 2. The efficiently selected stencil does not necessarily contain all the sampling points on one side of the discontinuity.

A solution-based refinement measure e_j is derived for SSC in (Witteveen & Iaccarino 2011*a*,*c*) based on the probability $\bar{\Omega}_j$, size $\bar{\Xi}_j$, and polynomial degree p_j of simplex Ξ_j. The impact of the stencil selection on the increase of p_j in the smooth regions of the solution decreases the measure e_j in the simplexes in which the solution is smooth. This results for SSC–ENO in more focused refinement of the simplexes that contain nonlinearities. For more details the reader is referred to (Witteveen & Iaccarino 2011*b*).

4. Subcell resolution

Adaptive refinement and linear interpolation require a sufficient number of samples to approximate discontinuities accurately. In problems with spatial discontinuities, the deterministic solutions $v_k(x)$ for the samples $\boldsymbol{\xi}_k$ already contain information about the location of the discontinuity $\boldsymbol{\xi}_{\text{disc}}$ in probability space. We use this observation to derive a relation for $\boldsymbol{\xi}_{\text{disc}}$ as a function of the spatial coordinate x by extracting the discontinuity locations v_{disc_k} in physical space from $v_k(x)$. The interpolations $w_j(\boldsymbol{\xi})$ in the continuous cells Ξ_j are then extrapolated into the cells in probability space that contain the discontinuity up to its estimated location $\boldsymbol{\xi}_{\text{disc}}$. This subcell resolution approach does not require adaptive refinement and linear interpolation to approximate discontinuities. SSC–SR obtains a higher-degree interpolation in the entire probability space in combination with a sharp resolution of the jump for response surfaces with an *a priori* unknown discontinuity location.

In problems with one spatial dimension, the discontinuity location v_{disc_k} in physical space is first extracted from the deterministic solutions $v_k(x)$ for the samples $\boldsymbol{\xi}_k$. These realizations v_{disc_k} are then interpolated using the SSC–ENO algorithm to a function $w_{\text{disc}}(\boldsymbol{\xi})$ describing the discontinuity location in physical space as a function of the uncertain parameters $\boldsymbol{\xi}$. The discontinuity location in the response surface $w(\boldsymbol{\xi})$ in probability space for a certain x–location in physical space is given by $\boldsymbol{\xi}_{\text{disc}} \in \Xi$ for which

$$w_{\text{disc}}(\boldsymbol{\xi}_{\text{disc}}) = x, \tag{4.1}$$

holds. The response surface interpolation $w_j(\boldsymbol{\xi})$ of the samples v_k at that x–location is constructed in the cells Ξ_j that do not contain the discontinuity location $\boldsymbol{\xi}_{\text{disc}}$, using the SSC–ENO algorithm as in Section 3. In the other cells, the linear approximation is replaced by the extension of the interpolations $w_j(\boldsymbol{\xi})$ in the neighboring cells Ξ_j from both sides up to $\boldsymbol{\xi}_{\text{disc}}$. If the interpolation $w_{\text{disc}}(\boldsymbol{\xi})$ is continuous in $\boldsymbol{\xi}$, then the discontinuity location $\boldsymbol{\xi}_{\text{disc}}$ also varies continuously with x. The discontinuity location consists of a set Ξ_{disc} of points $\boldsymbol{\xi}_{\text{disc}} \in \Xi_{\text{disc}} \subset \Xi$ in the case of multiple uncertain parameters $\boldsymbol{\xi}$. In multiple spatial dimensions, the distance from the discontinuity to a point $\mathbf{x}$ in physical space is parameterized, instead of the location of the discontinuity. Regular perturbation problems have been considered so far, without topological changes such as merging or emerging discontinuities in probability space.

5. Shock tube problem

The effectiveness of the developed approaches for resolving uncertain spatial discontinuities is tested on a shock tube problem. The results of the SSC method, SSC–ENO, and SSC–SR are compared with the deterministic solution.

5.1. *Sod's Riemann problem in a closed shock tube*

The shock tube problem involves Sod's standard Riemann problem for the Euler equations of one-dimensional unsteady inviscid flow without heat conduction. This problem was also used by Poëtte *et al.* (2009) and Tryoen *et al.* (2010) for uncertainty analysis of an example with steep fronts and shocks. The governing system of hyperbolic equations is given in conservation form by

$$\frac{\partial U}{\partial t} + \frac{\partial F(U)}{\partial x} = 0, \qquad U = \begin{pmatrix} \rho \\ \rho u \\ \rho E \end{pmatrix}, \qquad F = \begin{pmatrix} \rho u \\ \rho u^2 + p \\ \rho u H \end{pmatrix}, \tag{5.1}$$

with the state vector $U(x,t)$, the flux vector $F(x,t)$ and the initial conditions $U(x,0) = U_0(x)$. For a perfect gas, the density $\rho(x,t)$, velocity $u(x,t)$, static pressure $p(x,t)$, total specific energy $E(x,t)$, and total specific enthalpy $H(x,t)$ are related as $E = (1/(\gamma - 1))p/\rho + u^2/2$ and $H = E + p/\rho$, with the adiabatic coefficient $\gamma = c_{\text{p}}/c_{\text{v}}$. Sod's Riemann problem is characterized by the initial conditions $U_0(x)$ consisting of two uniform states at the left and right sides of x_0 with $(u_{\text{left}}; p_{\text{left}}; \rho_{\text{left}}) = (0; 1; 1)$ and $(u_{\text{right}}; p_{\text{right}}; \rho_{\text{right}}) = (0; 0.1; 0.125)$. The problem is here confined to a closed shock tube on a finite spatial domain $x \in [-0.2; 2]$ with reflective walls at the boundaries.

The pressure p_{left} of the initial left state and the location x_0 of the initial discontinuity are uncertain, given by two uncorrelated uniform distributions on the domains $p_{\text{left}} \in [0.9; 1.1]$ and $x_0 \in [-0.025; 0.025]$. The output quantities of interest are the response surface of ρ at $x = 0.82$, and its statistical moments and confidence intervals on the entire spatial domain. The Euler equations (5.1) are solved up to $t = 1$ using a second-order front tracking method (Witteveen 2010), which resolves shock waves and contact surfaces as true discontinuities. The space-time solution of the deterministic problem is shown in Figure 5 in terms of the wave paths for $n_{\text{f}} = 16$ fronts discretizing the rarefaction fan. The corresponding profile of ρ at $t = 1$ is given in Figure 6 for $n_{\text{f}} = 64$.

5.2. *Uncertain density at* $x = 0.82$

The uncertainty in p_{left} and x_0 leads to a jump in the response surface for the density ρ at an x–location near the contact discontinuity, $x = 0.82$. The SSC discretization of

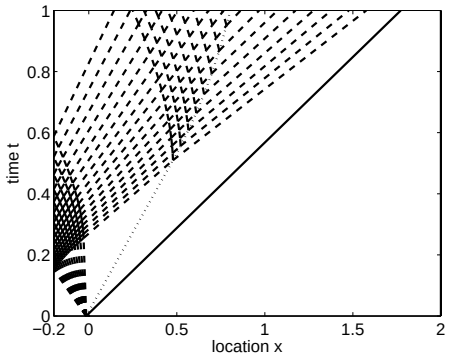

FIGURE 5. Deterministic space-time solution with $n_\mathrm{f} = 16$: shock wave (full line); characteristics (dashed line); contact discontinuity (dotted line).

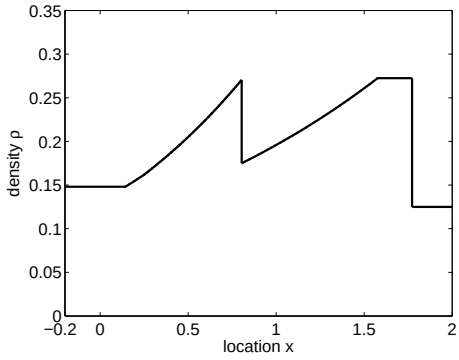

FIGURE 6. Deterministic density profile ρ at $t = 1$ with $n_\mathrm{f} = 64$.

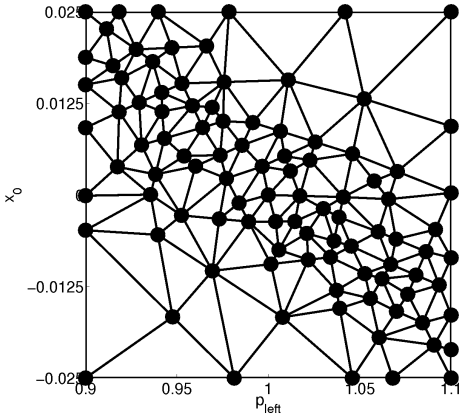

FIGURE 7. SSC discretization of probability space for the density ρ at $x = 0.82$ and $t = 1$ with $n_\mathrm{s} = 100$.

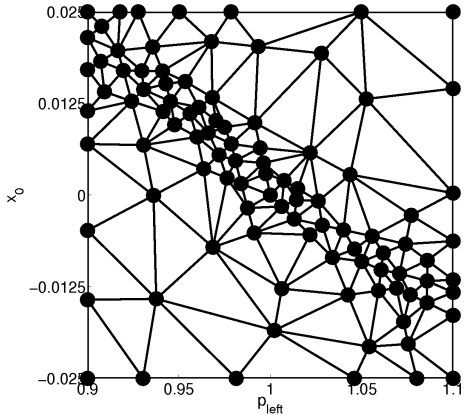

FIGURE 8. SSC–ENO discretization of probability space for the density ρ at $x = 0.82$ and $t = 1$ with $n_\mathrm{s} = 100$.

the two-dimensional probability space is shown in Figure 7 in terms of the tessellation of $n_\mathrm{s} = 100$ sampling points. The adaptive refinement algorithm clusters the sampling points near the discontinuity that runs diagonally through the probability space. The SSC–ENO method obtains a significantly higher density of the sampling points near the jump in Figure 8 for the same number of samples. This results in a sharper resolution of the discontinuity and a larger ratio in size between the cells near the singularity and those that discretize the continuous regions. The improved effectiveness of the adaptive refinement is caused by the increase of the local polynomial degree p_j in the smooth cells Ξ_j by the stencil selection and the resulting concentration of the sampling in the cells that contain the discontinuity. SSC–ENO predicts a mean pressure of $\mu_\rho = 0.231$ with a standard deviation of $\sigma_\rho = 0.0543$. The coarser discretization of the discontinuity by SSC leads to an underprediction of the standard deviation with $\sigma_\rho = 0.0534$.

The SSC–ENO response surface approximation for ρ as a function of p_left and x_0 with the simplex tessellation is shown in Figure 9. The response shows two continuous regions

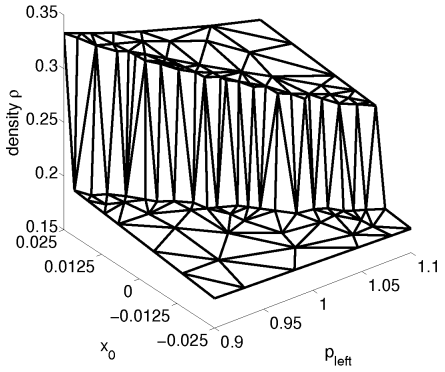

FIGURE 9. SSC–ENO response surface approximation for the density ρ at $x = 0.82$ and $t = 1$ with $n_s = 100$.

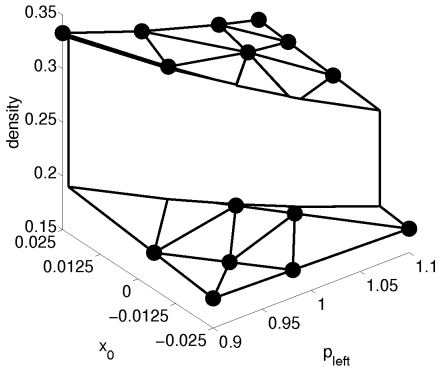

FIGURE 10. SSC–SR response surface approximation for the density ρ at $x = 0.82$ and $t = 1$ with $n_s = 15$.

separated by a discontinuity that varies in strength and that is slightly curved. SSC–ENO gives a robust approximation of the discontinuity without overshoots because of the linear interpolation in the small simplexes that contain the singularity. Nevertheless, the subcell resolution of the SSC–SR method already achieves a more accurate response surface approximation using uniform sampling with only $n_s = 15$ samples in Figure 10. The jump is captured as a true discontinuity by extrapolating the interpolations $w_j(\boldsymbol{\xi})$ from both sides into the discontinuous cells up to the predicted singularity location. This leads to a piecewise higher-degree approximation that resolves the two smooth regions and the curved discontinuity of varying strength in between.

The discontinuity location is approximated by interpolating the contact discontinuity locations x_{contact} extracted from the deterministic simulations, as shown in Figure 11. The interpolation of x_{contact} as a function of p_{left} and x_0 is performed using the SSC–ENO algorithm. The resulting jump line for $x = 0.82$ in the (p_{left}, x_0)–plane is then given by the intersection of the surface for x_{contact} with the horizontal plane at $x_{\text{contact}} = 0.82$. The jump line approximation consists of a piecewise higher-order polynomial that is able to capture its curvature. The statistical moments predicted by SSC–SR are $\mu_\rho = 0.231$ and $\sigma_\rho = 0.0557$. The mean value matches that of SSC–ENO, but the standard deviation is underpredicted by SSC–ENO because of the linear approximation of the discontinuity. It corresponds to an output coefficient of variation of $\text{CoV}_\rho = 24.1\%$.

5.3. *Uncertain density field*

The output uncertainty in the entire density profile on $x \in [-0.2; 2]$ is depicted in Figure 12 in terms of the 90% and 100% confidence intervals compared to the mean density profile for SSC–SR with $n_s = 15$. The variation in the discontinuity locations is captured by the 100% interval, which is broadest in these regions and asymmetrical around the mean caused by the highly nonlinear propagation of the input uncertainty. The interval around the shock wave shows the robust approximation without overshoots at the discontinuity. The varying interval size near the contact surface is caused by the physical variation of the density jump strength in the interaction region. There is no uncertainty at the right boundary because the region at the right of the shock wave lies outside the domain of influence of p_{left} and x_0.

The convergence of the mean μ_ρ and the standard deviation σ_ρ is shown in Figures 13

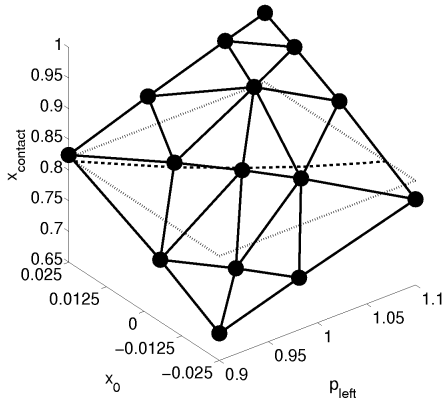

FIGURE 11. SSC–SR response surface approximation for the location of the contact discontinuity x_{contact} at $t = 1$ with $n_{\text{s}} = 15$.

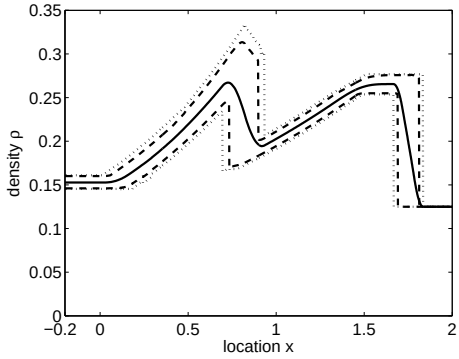

FIGURE 12. SSC–SR solution for the mean (full line), and 90% (dashed line) and 100% (dotted line) uncertainty intervals of the density ρ at $t = 1$ with $n_{\text{s}} = 15$.

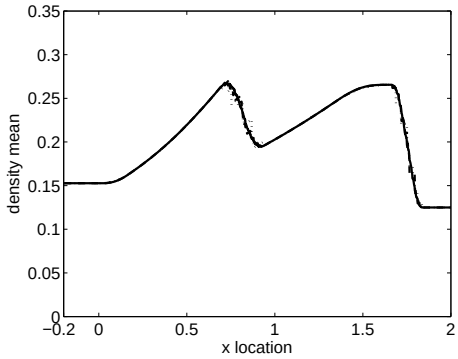

FIGURE 13. SSC–ENO solution for the mean μ_ρ of the density ρ at $t = 1$: $n_{\text{s}} = 10$ (dotted line); $n_{\text{s}} = 20$ (dashed line); $n_{\text{s}} = 100$ (full line).

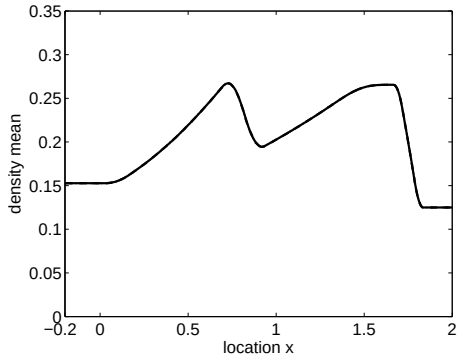

FIGURE 14. SSC–SR solution for the mean μ_ρ of the density ρ at $t = 1$: $n_{\text{s}} = 10$ (dotted line); $n_{\text{s}} = 15$ (dashed line); $n_{\text{s}} = 20$ (full line).

to 16. The solutions of SSC–ENO with $n_{\text{s}} = \{10, 20, 100\}$ samples are compared with those of SSC–SR with $n_{\text{s}} = \{10, 15, 20\}$. SSC–ENO with uniform refinement is used here, since adaptive refinement is not effective for spatial domains with uncertain discontinuity locations. The staircase character of the SSC–ENO approximation near the discontinuities shows the challenge of representing these spatial uncertainties. The solution changes only when the discontinuity in probability space crosses a sampling point, which results in the series of steps. With an increasing number of samples, the solution converges to a smooth representation with a larger number of smaller jumps. However, due to the absence of viscosity in the physical problem, the approximation maintains a staircase character which leads to first-order accuracy. It also results in the convergence to the standard deviation from below, which causes an underprediction of the maximum standard deviation at underresolved sample sizes.

The SSC–SR solutions for μ_ρ and σ_ρ are smooth functions of x because the subcell resolution results in a continuous variation of the discontinuity location with x. The

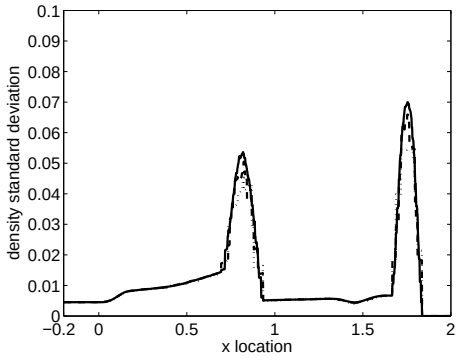

FIGURE 15. SSC–ENO solution for the standard deviation σ_ρ of the density ρ at $t = 1$: $n_s = 10$ (dotted line); $n_s = 20$ (dashed line); $n_s = 100$ (full line).

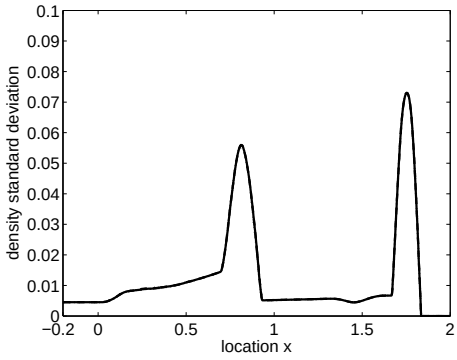

FIGURE 16. SSC–SR solution for the standard deviation σ_ρ of the density ρ at $t = 1$: $n_s = 10$ (dotted line); $n_s = 15$ (dashed line); $n_s = 20$ (full line).

mean density shows the smearing of the shock and contact waves compared to the deterministic solution, which is caused by the effect of the uncertainty on the location of the discontinuities. This also produces the local maxima of the standard deviation in the discontinuous regions. The results for $n_s = \{10, 15, 20\}$ are indistinguishable and converged to a maximum standard deviation of $\sigma_{\rho,\max} = 0.0730$ at $x = 1.754$ for $n_s = 15$. SSC–ENO underestimates the maximum output uncertainty with $\sigma_{\rho,\max} = 0.0700$ by 4.16% even for $n_s = 100$.

The confidence interval is shown in Figure 12 in terms of the 90% and 100% uncertainty bars compared to the mean density profile for SSC–SR with $n_s = 15$. The variation in the discontinuity locations is captured by the 100% interval, which is broadest in these regions and asymmetrical around the mean caused by the highly nonlinear propagation of the input uncertainty. The interval around the shock wave shows the robust approximation without overshoots at the discontinuity. The varying interval size near the contact surface is caused by the physical variation of the density jump strength in the interaction region. There is no uncertainty at the right boundary because the region at the right of the shock wave lies outside the domain of influence of p_{left} and x_0.

Acknowledgments

This work was supported by the Netherlands Organization for Scientific Research (NWO) and the European Union Marie Curie Cofund Action under Rubicon grant 680-50-1002.

REFERENCES

ABGRALL, R. 2010 A simple, flexible and generic deterministic approach to uncertainty quantifications in nonlinear problems: application to fluid flow problems. In *5th European Conference on Computational Fluid Dynamics, ECCOMAS CFD, Lisbon, Portugal*.

AGARWAL, N. & ALURU, N. R. 2009 A domain adaptive stochastic collocation approach for analysis of MEMS under uncertainty. *J. Comput. Phys.* **228**, 7662–7688.

BABUŠKA, I., NOBILE, F. & TEMPONE, R. 2007 A stochastic collocation method for

elliptic partial differential equations with random input data. *SIAM J. Numer. Anal.* **45**, 1005–1034.

Babuška, I., Tempone, R. & Zouraris, G. E. 2004 Galerkin finite elements approximation of stochastic finite elements. *SIAM J. Numer. Anal.* **42**, 800–825.

Barth, T. 2011*a* On the propagation of statistical model parameter uncertainty in CFD calculations. *Theor. Comput. Fluid Dyn.* DOI: 10.1007/s00162-011-0221-2.

Barth, T. 2011*b* UQ methods for nonlinear conservation laws containing discontinuities. In *AVT–193 Short Course on Uncertainty Quantification, Stanford, California*.

Foo, J., Wan, X. & Karniadakis, G. E. 2008 The multi-element probabilistic collocation method (ME–PCM): error analysis and applications. *J. Comput. Phys.* **227**, 9572–9595.

Ghanem, R. G. & Spanos, P. D. 1991 *Stochastic finite elements: a spectral approach*. Springer–Verlag, New York.

Ghosh, D. & Ghanem, R. 2008 Stochastic convergence acceleration through basis enrichment of polynomial chaos expansions. *Int. J. Numer. Meth. Eng.* **73**, 162–184.

Harten, A. 1989 ENO schemes with subcell resolution. *J. Comput. Phys.* **83**, 148–184.

Harten, A. & Osher, S. 1987 Uniformly high-order accurate nonoscillatory schemes I. *SIAM J. Numer. Anal.* **24**, 279–309.

Le Maître, O. P., Najm, H. N., Ghanem, R. G. & Knio, O. M. 2004 Multi-resolution analysis of Wiener-type uncertainty propagation schemes. *J. Comput. Phys.* **197**, 502–531.

Ma, X. & Zabaras, N. 2009 An adaptive hierarchical sparse grid collocation algorithm for the solution of stochastic differential equations. *J. Comput. Phys.* **228**, 3084–3113.

Poëtte, G., Després, B. & Lucor, D. 2009 Uncertainty quantification for systems of conservation laws. *J. Comput. Phys.* **228**, 2443–2467.

Shu, C.-W. & Osher, S. 1988 Efficient implementation of essentially non-oscillatory shock-capturing schemes. *J. Comput. Phys.* **77**, 439–471.

Tryoen, J., Le Maître, O., Ndjinga, M. & Ern, A. 2010 Intrusive Galerkin methods with upwinding for uncertain nonlinear hyperbolic systems. *J. Comput. Phys.* **229**, 6485–6511.

Wan, X. & Karniadakis, G. E. 2005 An adaptive multi-element generalized polynomial chaos method for stochastic differential equations. *J. Comput. Phys.* **209**, 617–642.

Witteveen, J. A. S. 2010 Second order front tracking for the Euler equations. *J. Comput. Phys.* **229**, 2719–2739.

Witteveen, J. A. S. & Iaccarino, G. 2011*a* Refinement criteria for simplex stochastic collocation with local extremum diminishing robustness. Submitted.

Witteveen, J. A. S. & Iaccarino, G. 2011*b* Simplex stochastic collocation with ENO-type stencil selection for robust uncertainty quantification. Submitted.

Witteveen, J. A. S. & Iaccarino, G. 2011*c* Simplex stochastic collocation with random sampling and extrapolation for non-hypercube probability spaces. Submitted.

Xiu, D. & Hesthaven, J. S. 2005 High-order collocation methods for differential equations with random inputs. *SIAM J. Sci. Comput.* **27**, 1118–1139.

Xiu, D. & Karniadakis, G. E. 2002 The Wiener–Askey polynomial chaos for stochastic differential equations. *SIAM J. Sci. Comput.* **24**, 619–644.